Acta Cryst. (1990). A**46**, 799-809

Defect Structure of Zirconia ($Zr_{0.85}Ca_{0.15}O_{1.85}$) at 290 and 1550 K

BY R. B. NEDER, F. FREY AND H. SCHULZ

Institut für Kristallographie und Mineralogie, Theresienstrasse 41, 8000 *München* 2, *Federal Republic of Germany*

(*Received* 3 *August* 1989; *accepted* 25 *May* 1990)

Abstract

A quantitative interpretation of diffuse neutron scattering has yielded an accurate description of the defect structure of CaO stabilized zirconia (CSZ) at 290 and 1550 K. The defect structure is based on the correlated distribution of two different types of microdomains within the disordered structure. The first microdomain is built around a single oxygen vacancy with relaxed neighboring ions. The first neighbors are relaxed along ⟨100⟩, second neighbors are relaxed along ⟨111⟩ and ⟨110⟩. The second microdomain is built around a pair of oxygen vacancies separated by $a3^{1/2}/2$ along ⟨111⟩ with a Ca ion in between. There is no qualitative change at high temperatures. The correlation length, however, decreases considerably.

Introduction

Cubic zirconia crystallizes in the fluorite structure, space group $Fm3m$, with zirconium on $4(a)$ $(0, 0, 0)$ and oxygen on $8(f)$ $(\frac{1}{4}, \frac{1}{4}, \frac{1}{4})$. It is generally accepted that the dopant ions used to stabilize the cubic structure occupy the zirconium position and that vacancies are introduced on the oxygen site (Subbarao, 1981).

Defect structures of cubic zirconia have been the object of several investigations. Nevertheless, a conclusive result has not yet been obtained. Two different models are proposed. On the one hand, a homogeneous crystal is assumed with cooperative displacement of the oxygen ions (Carter & Roth, 1963; Steele & Fender, 1974; Faber, Mueller & Cooper, 1978; Morinaga, Cohen & Faber, 1979, 1980; Horiuchi, Schultz, Leung & Williams, 1984), on the other, a distribution of microdomains of an ordered phase within the crystal is proposed (Allpress & Rossell, 1975; Allpress, Rossell & Scott, 1975; Hudson & Moseley, 1976; Andersen, Clausen, Hackett, Hayes, Hutchings, Macdonald & Osborn, 1985, 1986; Osborn, Andersen, Clausen, Hackett, Hayes, Hutchings & Macdonald, 1985). A comparison of the results is made more difficult because different compositions were examined that had been subjected to different annealing histories.

Carter & Roth (1963) proposed an order-disorder phase transition for CSZ. In the ordered phase the oxygen ions are displaced along ⟨111⟩ by about 0·02 nm. They found a strongly modulated background and diffuse satellites for the samples that had been annealed at 1370 K. Steele & Fender (1974) interpreted the background modulation in neutron powder diagrams of yttrium-stabilized zirconia (YSZ) by a displacement of the oxygen ions along ⟨100⟩ by 0·036 nm. Faber, Mueller & Cooper (1978) confirmed these results. For both YSZ and CSZ they found a displacement along ⟨100⟩ by 0·022 nm. They did not report diffuse scattering. Morinaga, Cohen & Faber (1979, 1980) examined both YSZ and CSZ by X-ray diffraction. From their interpretation of the Bragg intensities and the diffuse scattering they concluded a displacement along ⟨111⟩ by 0·044 nm for both YSZ and CSZ. Horiuchi *et al.* (1984) reported displacement along ⟨111⟩, as well as ⟨100⟩. They interpreted the displacement along ⟨111⟩ by split positions as a model for large anharmonic vibrations, while the displacement along ⟨100⟩ is a static displacement of the oxygen ions. Lorenz, Frey, Schulz & Boysen (1988) confirmed the anharmonic nature of the thermal vibrations by refinement of the Debye-Waller factors obtained from a single-crystal neutron diffraction data set at 1170, 1370 and 1770 K.

Allpress & Rossell (1975) observed diffuse scattering that changed little with change of composition. By electron microscopy they observed an irregular contrast. They concluded that the crystal contains microdomains within the disordered matrix. They suggested that the microdomains have a structure similar to the structure of the Φ_1 phase reported for yttrium-stabilized hafnia (Allpress, Rossell & Scott, 1975), since the positions of the diffuse scattering roughly coincides with the positions of the Φ_1 reflections found in the hafnia compound. Morinaga, Cohen & Faber (1980) compared the observed diffuse intensity with the calculated intensity and concluded that the diffuse scattering cannot be caused by microdomains with a structure similar to that of the Φ_1 phase. In contrast to Allpress & Rossell (1975), Hudson & Moseley (1976) reported that the intensity of the diffuse scattering changes as the composition changes. They suggested that the microdomains might contain a cluster of the type which Thornber, Bevan & Graham (1968) described. This cluster is based on two anion vacancies separated by $a3^{1/2}/2$ along ⟨111⟩. Andersen *et al.* (1985, 1986) and Osborn *et al.* (1985)

0108-7673/90/100799-11$03.00

found that the diffuse scattering in YSZ can be indexed by satellite vectors $\pm(0{\cdot}4\,0{\cdot}4\,\pm0{\cdot}8)$. They describe the defect structure by the cluster suggested by Hudson & Moseley (1976). The oxygen ions are relaxed along ⟨100⟩ towards the vacancies and the cations are relaxed along ⟨111⟩ away from the vacancies. With this model they obtain reasonable agreement of the calculated and observed intensity distribution. Hull *et al.* (1988) extended the work by Andersen *et al.* (1985, 1986) and Osborn *et al.* (1985) to high temperatures. They found a dynamic behavior of the vacancies and possibly smaller aggregates at 2780 K.

Butler, Catlow & Fender (1983) calculated the lattice energies for the two different models. They reported that both models have nearly identical energies with the microdomain model being favored by 0·09 eV per dopant ion. They conclude that both types may coexist in the structure.

In this study the diffuse neutron intensity of cubic zirconia was measured at room temperature and at 1550 K. The observed intensity is interpreted by a model of correlated microdomains. This model assumes the following conditions. Embedded in an otherwise disordered crystal of cubic zirconia one or several different microdomains are coherently intergrown. These microdomains are defects based on oxygen vacancies and the relaxed surrounding. The distribution of these microdomains shows short-range order. The theory of diffuse scattering by correlated microdomains is described by Neder, Frey & Schulz (1990).

Experimental

The single crystals used in this study, grown by the skull melting method, were provided by Djevahirdjan S.A., Monthey, Switzerland. The sample size was about $20\times20\times50$ mm. A chemical analysis by spectral analysis (ICP) yielded a composition of 15 ± 1 mol % CaO. The size of the original crystal was sufficient for a cube of $11\times11\times11$ mm to be cut, on one side of which a stem of $2\times2\times40$ mm was left, Fig. 1. The stem was fixed to an Al_2O_3 rod of 2 mm diameter by a ceramic glue based on ZrO_2. To avoid spurious scattering the ceramic glue was surrounded by a cylinder of BN, Fig. 1. This novel approach to the crystal support enabled a measurement of the diffuse scattering that was free from any background due to the crystal holder.

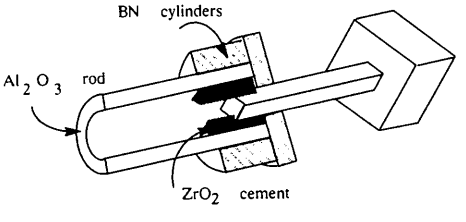

Fig. 1. Shape of sample and sample holder. The stem of the sample crystal is connected to the Al_2O_3 rod by ZrO_2 cement. Two BN cylinders serve to absorb the intensity scattered by the cement.

The experiments were carried out at the neutron spectrometer MAN II at the research reactor in Garching (FRM), Federal Republic of Germany. The wavelength used was 1·2 Å. The intensity of $\lambda/2$ was about 2% of the intensity of the main wavelength and the observed scattered intensity was corrected accordingly.

For the high-temperature measurements a mirror furnace developed by Lorenz (1988) was used. This furnace operates under normal atmosphere and yields temperatures up to 2000 K.

Measurements

For the room-temperature measurements an as-grown crystal was used. No further heat treatment was applied. The following layers in reciprocal space were measured in the integral mode of the diffractometer, *i.e.* without analyzer:

(I) the zero layer of the [1, −1, 0] zone (Fig. 2);

(II) second layer of the [1, −1, 0] zone (Fig. 3);

(III) zero layer of the [0, −1, 0] zone (Fig. 4);

(IV) a section of the [1, −1, 0] zone around 114 from (*hkl*) $[1,-1,0]=-0{\cdot}4$ to $+1{\cdot}2$ in steps of 0·2 (Fig. 5).

All layers were scanned in steps of 0·05 reciprocal-lattice constants in ⟨110⟩ and ⟨001⟩ directions.

In both layers of the [1, −1, 0] zone, two different diffuse-scattering phenomena can be observed. In the zero layer, Fig. 2, broad bands of diffuse intensity reach from 440 to 333 and further to 004. In the second layer, Fig. 3, a band reaches from 531 to the forbidden 314. These bands do not show a constant

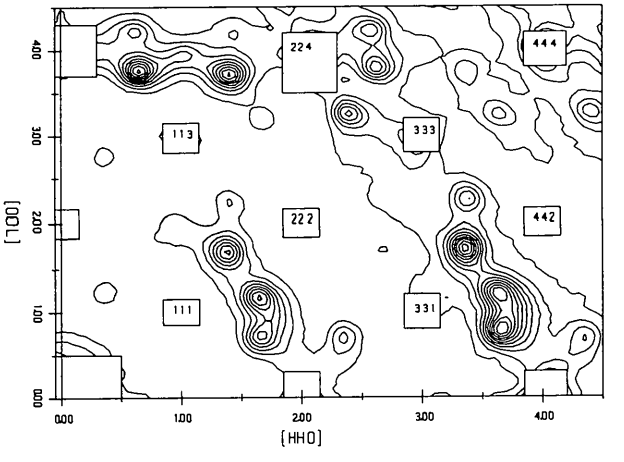

Fig. 2. Zero layer of the [1, −1, 0] zone, $T=290$ K. The intensities are stepped with linear intervals of 50 counts, the lowest intensity represented is 100 counts. The Bragg reflections are represented by the rectangles.

2Θ and, thus, they are not powder diffraction rings. The second phenomena are diffuse peaks that can be indexed as satellites with diffraction vectors of $\pm(0{\cdot}4\ 0{\cdot}4 \pm 0{\cdot}8)$. The FWHM of these diffuse peaks is about 0·25 reciprocal-lattice constants. The length of the superstructure vector corresponds to a correlation length of 0·52 nm and the FWHM corresponds to a coherence length of 2·0 nm. The measurements of the sections of the [1, −1, 0] zone around 114, Fig. 5, show that the peak intensity of the diffuse peaks lies exactly in the zero layer of [1, −1, 0] and that the FWHM is the same in all directions.

At 1550 K the following layers were measured by the same step scanning mode:

(I) zero layer [1, −1, 0] zone, purely elastic intensity (Fig. 6);

(II) zero layer [1, −1, 0] zone, integral intensity (Fig. 7).

Both measurements show qualitatively the same scattering effects as the room-temperature measurements. The FWHM of the diffuse peaks, however, is enlarged to 0·30 reciprocal-lattice constants. In particular, the integral measurement shows that the intensity of the diffuse peaks is much lessened in comparison to the broad bands. This indicates a different origin for the two phenomena. The elastic

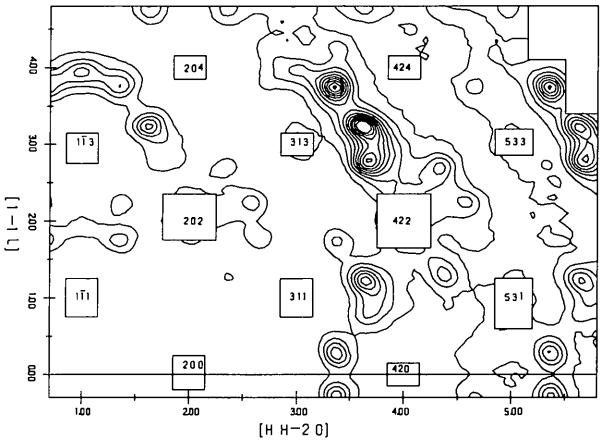

Fig. 3. First layer of the [1, −1, 0] zone, $T = 290$ K. The intensities are stepped with linear intervals of 50 counts, the lowest intensity represented is 100 counts. The Bragg reflections are represented by the rectangles.

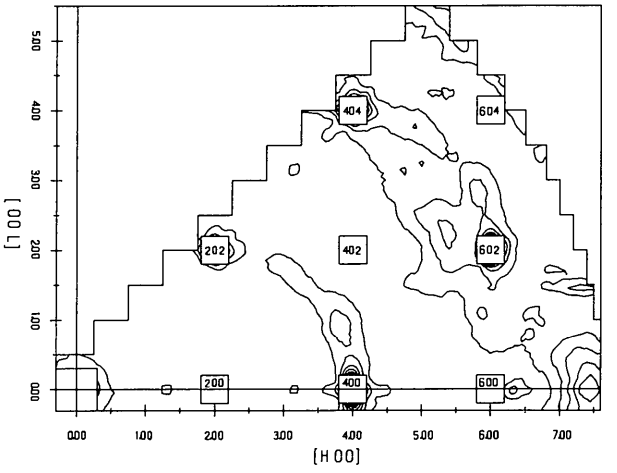

Fig. 4. Zero layer of the [0, −1, 0] zone, $T = 290$ K. The intensities are stepped with linear intervals of 50 counts, the lowest intensity represented is 100 counts. The Bragg reflections are represented by the rectangles.

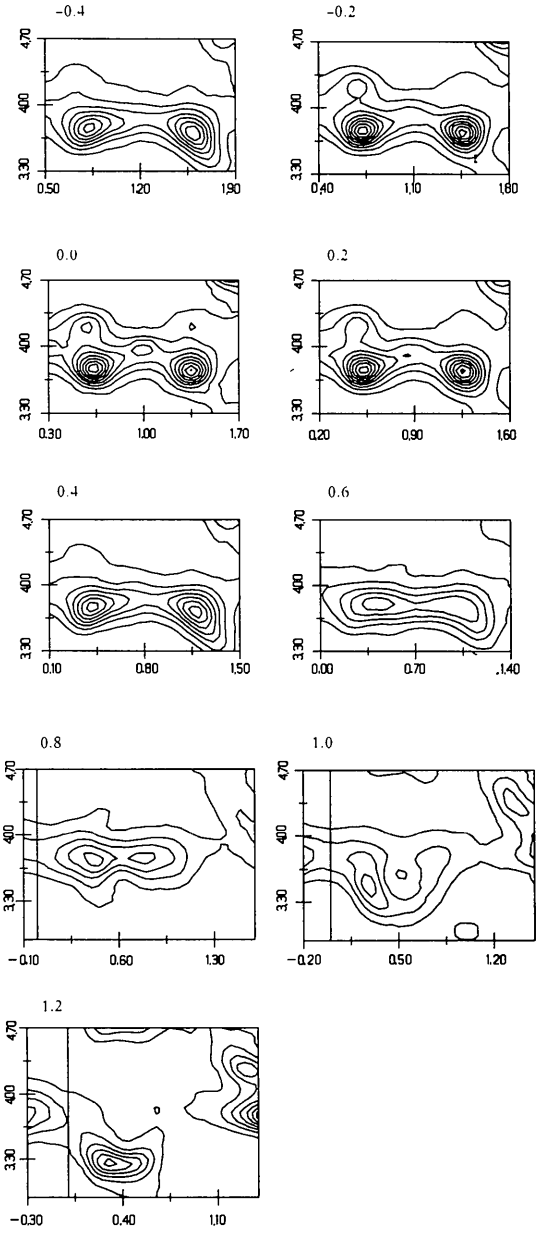

Fig. 5. Section of the [1, −1, 0] zone from (*hkl*) [1, −1, 0] = −0·4 to +1·2 in steps of 0·2, $T = 290$ K. The intensities are stepped with linear intervals of 50 counts, the lowest intensity represented is 100 counts.

and the integral measurements do not show any substantial differences within the instrumental resolution of 0·242 THz. Thus it is shown that the diffuse scattering is due to a static disorder or is quasielastic within the instrumental resolution.

The phase diagram by Hellmann & Stubican (1983) shows that the high-temperature measurements were carried out within the field of stability of the cubic phase. Thus, for the first time, it has been proven that even at these high temperatures the stable calcium-stabilized cubic phase contains correlated defects.

After quenching the sample from 1550 K to room temperature, sections of the zero layer of the [1, −1, 0] zone were measured by the elastic setting of the diffractometer. These measurements do not show a new type of scattering phenomenon. The intensity is the same as that observed before the heating. During the quenching process no new defect types develop. Therefore, the type of defect structure is preserved, while the length of coherence increases. This process is reversible.

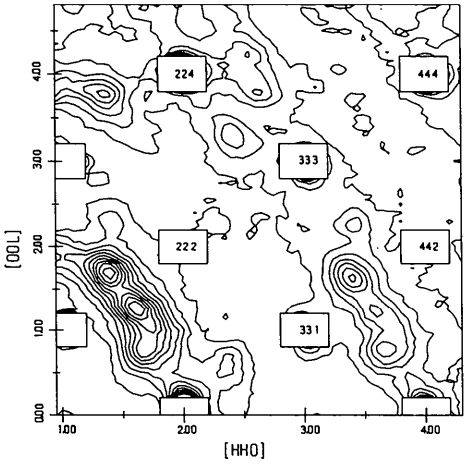

Fig. 6. Zero layer of [1, −1, 0] zone, $T = 1550$ K, elastic intensity. The intensities are stepped with linear intervals of 10 counts, the lowest intensity represented is 20 counts. The Bragg reflections are represented by the rectangles.

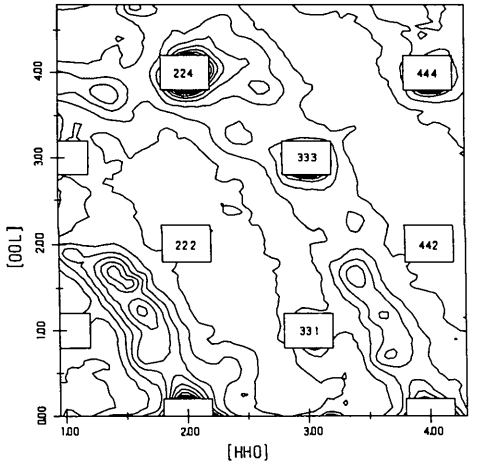

Fig. 7. Zero layer of the [1, −1, 0] zone, $T = 1550$ K, integral intensity. The intensities are stepped with linear intervals of 50 counts, the lowest intensity represented is 100 counts. The Bragg reflections are represented by the rectangles.

Model

This section describes all types of microdomain that are based on the ideal fluorite structure. The microdomain proposed by Allpress & Rossell (1975) and Hudson & Moseley (1976) is based on the Φ_1 structure. Andersen *et al.* (1986) described a microdomain based on a pair of oxygen vacancies.

The basic type of microdomain is based on a single oxygen vacancy whose next neighbors are relaxed (Fig. 8). The symmetry of the coordination polyhedron suggests oxygen relaxation along ⟨100⟩. The four cation neighbors are relaxed along ⟨111⟩ away from the vacancy. To obtain charge neutrality one cation can be expected to be calcium. Since the ionic radius of calcium of 0·112 nm (Shannon, 1976) is larger than the radius of zirconium (0·084 nm), relaxation of the oxygen neighbors of the second sphere surrounding the calcium ion can be expected along ⟨111⟩ and ⟨110⟩.

Four modifications of this basic model were considered:

(*A*I) one calcium neighbor, O(1) relaxed along ⟨100⟩, O(2) relaxed along ⟨100⟩, O(3) relaxed along ⟨111⟩, O(4) relaxed along ⟨101⟩;

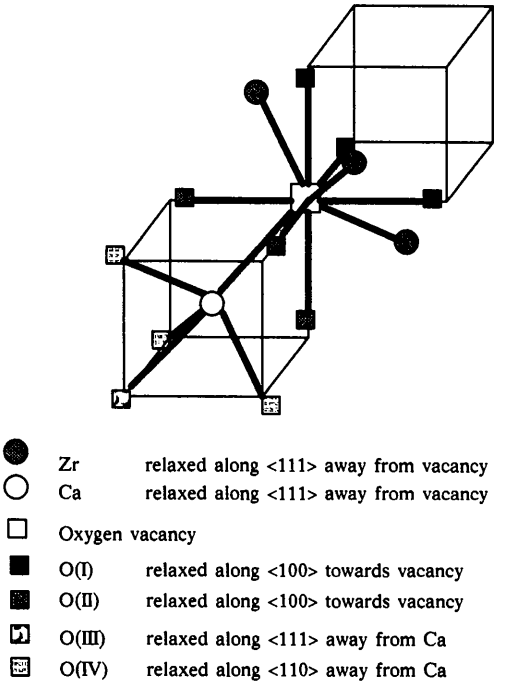

Fig. 8. Structure of the microdomains of type *A*. The microdomain is based on a single vacancy on the oxygen sublattice. The next neighbors are relaxed from their ideal positions.

(*A*II) one calcium neighbor, O(1) relaxed along ⟨100⟩, O(2) relaxed along ⟨211⟩, O(3) relaxed along ⟨111⟩, O(4) relaxed along ⟨101⟩;

(*A*III) one calcium neighbor, O(1) relaxed along ⟨100⟩, O(2) relaxed along ⟨100⟩, O3 relaxed along ⟨111⟩, O(4) relaxed along ⟨111⟩;

(*A*IV) only zirconium neighbors, O(1) relaxed along ⟨100⟩, O(2) relaxed along ⟨100⟩, O(3) and O(4) relaxed along ⟨111⟩.

In the microdomain *A*I the relaxation of O(2) is assumed in ⟨100⟩. Since the ionic radius of calcium is much larger than the radius of zirconium, the model *A*II allowed for an additional relaxation of the O(2) along ⟨111⟩ away from the calcium position to result in a relaxation along ⟨211⟩. For the same reason, the model *A*III allowed the relaxation of the O(4) along ⟨111⟩. In the defect structure of the Φ_1 phase the calcium ions are next-nearest neighbors to the oxygen vacancy. Therefore, the model *A*IV assumes a microdomain in which only zirconium ions are present as nearest neighbors to the oxygen vacancy.

The second type of microdomain is based on a pair of oxygen vacancies. These vacancies can be separated by:

(*B*I) $a/2$ along ⟨100⟩;

(*B*II) $a/2^{1/2}$ along ⟨110⟩;

(*B*III) $a3^{1/2}/2$ along ⟨111⟩ with a cation in between (Fig. 9);

(*B*IV) $a3^{1/2}/2$ along ⟨111⟩ without a cation in between.

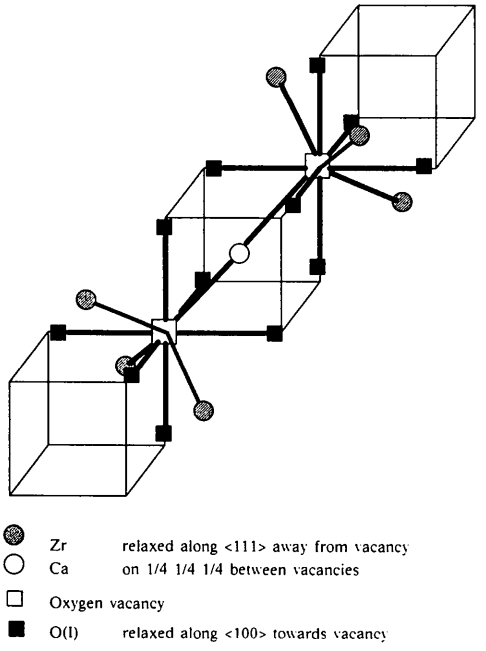

Fig. 9. Structure of the microdomain of type *B*III. The microdomain is based on a pair of vacancies on the oxygen sublattice separated by $a/2^{1/2}$ along [111]. The next neighbors are relaxed from their ideal positions.

The direction of relaxation is indicated in the figure by the displacement of the atoms. The next oxygen neighbors are relaxed along ⟨100⟩, the second neighbors are relaxed along ⟨111⟩. The orientation of each microdomain is defined by the orientation of the vector between the two vacancies.

The direction of the vector Ca–vacancy is taken as the orientation of the microdomain. If one cation is a calcium, eight possible orientations for the microdomain will result. In the following discussion, the orientation relationship between two microdomains is described by the relative orientation of their respective Ca–vacancy vectors. Two microdomains are said to be parallel if their respective Ca–vacancy vectors are parallel. In the calculations that follow, five different correlation schemes are tested. In the first scheme, the next neighbor of a microdomain is allowed to adopt any of the eight possible orientations, in the second, the first neighbor is restricted to the parallel orientation, in the third, the first neighbor is restricted to any but the parallel orientation. In the fourth scheme, the first neighbor is restricted to the parallel orientation and those three orientations that form an angle of 54·7° with the orientation of the original microdomain. Thus, for a given microdomain of orientation [111] the orientation of the first neighbor can be [111], [$\bar{1}$11], [1$\bar{1}$1] or [11$\bar{1}$]. In the fifth scheme these four orientations were allowed to be next neighbors that point into the corners of a tetrahedron. This results in two uncorrelated sets of correlated microdomains, namely (1) [111], [$\bar{1}\bar{1}$1], [$\bar{1}$1$\bar{1}$] and [1$\bar{1}\bar{1}$], and (2) [$\bar{1}\bar{1}\bar{1}$], [11$\bar{1}$], [1$\bar{1}$1] and [$\bar{1}$11]. For the sake of brevity the five correlation schemes will be referred to as 'all', 'parallel', 'non-parallel', 'nearly parallel' and 'tetrahedral'.

Refinements

For all the models discussed the diffuse intensity was calculated according to the theory presented by Neder, Frey & Schulz (1990). The calculated intensity was fitted to the observed intensities by least squares and a weighted residual R factor was calculated. The refinement of a data set consisting of the complete layer resulted in positional-parameter values of zero. Therefore, the peak intensity of only those points in reciprocal space corresponding to the satellites with diffraction vectors of $\pm(0{\cdot}4\ 0{\cdot}4\ \pm0{\cdot}8)$ was used as data set for the fit. For the room-temperature measurements 86 data points were used and 30 each for the elastic and integral measurements at 1550 K. The refinement for $T = 1550$ K resulted in incorrect values for the diffuse intensity of scattering vectors other than the satellite vector. The data set was expanded by the intensity of those points in reciprocal space at distance $\pm(0{\cdot}2\ 0{\cdot}2\ \pm0{\cdot}8)$ from the Bragg reflections. These points provided the background of uncorrelated diffuse scattering. With this new data set the

refinement resulted in meaningful results. With the resulting position parameters the intensity was calculated for the complete layers that had been measured at the two temperatures.

The data used for the refinement only include the peak intensities of the diffuse peaks. No information on the shape of the diffuse peaks was included. The length of coherence could therefore not be fitted.

The following parameters were kept fixed: neutron wavelength 0·12 nm; lattice constant 0·513 nm (T = 290 K); 0·520 nm (T = 1550 K); neutron scattering lengths (Koester & Yelon, 1983) O: 0·580; Zr: 0·716; Ca: 0·490 (10^{-14} m); Debye–Waller factors calculated by Rietveld refinements (Marxreiter, 1988), room temperature, O: 1·00; Zr: 0·50; Ca: 0·50; at 1550 K, O: 4·50; Zr: 2·50; Ca: 2·50; background (counts per monitor); integral mode, T = 290 K: 50; purely elastic mode, T = 1550 K: 5; integral mode, T = 1550 K, background as a quadratic function of $|\mathbf{h}|$, defined by the background at $\mathbf{h}$ = (0 0 0) 75; $\mathbf{h}$ = (1 1 1) 75; $\mathbf{h}$ = (4 4 4) 150; discrete spacing of the microdomains [R_0 in equations (15) and (24) in Neder, Frey & Schulz 1990)]: 0·36 nm, *i.e.* $1/2\,d_{110}$; relative abundance of Ca,Zr: 15 mol % CaO.

The following parameters were refined:

(I) overall scale factor;

(II) positional parameters that describe the relaxation away from the position in the ideal fluorite structure in the direction given by each model.

Microdomains of type *B*:

(*a*) oxygen relaxation in ⟨100⟩;

(*b*) cation relaxation in ⟨111⟩;

microdomains of type *A*:

(*c*) O(I) relaxation in ⟨100⟩;

(*d*) O(II) relaxation in ⟨100⟩;

(*e*) O(III) relaxation in ⟨111⟩;

(*f*) O(IV) relaxation in ⟨111⟩;

(*g*) Zr relaxation in ⟨111⟩;

(*h*) Ca relaxation in ⟨111⟩.

Refinements of the room-temperature data were carried out for all microdomains described and for combinations of different microdomain types. The measured intensities were weighted with the square root of the observed intensity. The different calculations used the various directions of relaxation for the microdomains of types *A* and *B* and also allowed for different correlation schemes of the microdomains.

The first refinements were carried out to check whether a single microdomain type can explain the observed diffuse scattering. The microdomain of type *A*I was used as a starting model. The correlation schemes 'all', 'nearly parallel' and 'tetrahedral' were used. The refinements resulted in *R* factors of 0·50, 0·48 and 0·48, respectively, for the three correlation schemes. The calculated diffuse-intensity plots showed large deviations from the observed diffuse intensity distribution. The large *R* factors show that a single microdomain type *A* cannot explain the observed diffuse intensity.

Table 1. *Results of the refinements*

The table lists the *R* factors for the various refinements. Listed for each refinement are the type of microdomain used (single-vacancy microdomains of type *A*, double-vacancy microdomains of type *B*), the correlation schemes among the microdomains of type *A*, between the microdomains of type *A* and type *B* and among microdomains of type *B*.

Type of microdomain		Correlation schemes among microdomains: Single	Single–double	Double	*R* factor (%)
*A*I		All			49·6
*A*I		Nearly parallel			48·4
*A*I		Tetrahedral			48·4
	*B*I			All	60·0
	*B*II			All	51·7
	*B*III			All	49·3
	*B*IV			All	53·3
*A*I	*B*III	Nearly parallel	All	None	39·2
*A*I	*B*III	Nearly parallel	Parallel	None	27·0
*A*I	*B*III	Nearly parallel	Not parallel	None	56·2
*A*I	*B*III	All	Parallel	None	36·2
*A*I	*B*IV	Nearly parallel	Parallel	None	35·2
*A*I	*B*IV	All	Parallel	None	42·6
*A*II	*B*III	Nearly parallel	Parallel	None	31·4
*A*III	*B*III	Nearly parallel	Parallel	None	33·9
*A*IV	*B*III	Nearly parallel	Parallel	None	25·0

In the same way the four different microdomain models *B* were refined. Only the correlation scheme 'all' was used, since the refinements of the different correlation schemes with the microdomain type *A*I did not result in different *R* factors, nor in different values for the relaxation of the ions. The *R* factors for the refinement of the microdomains *B*I to *B*IV were 0·60, 0·52, 0·49 and 0·53, respectively, and the calculated diffuse intensity plots did not agree with the observed intensity.

These calculations showed that a single microdomain type does not describe the defect structure of CSZ. Neither the microdomain based on a single vacancy nor any of those based on a pair of vacancies could explain the observed intensities.

The next refinements used combinations of two microdomain types, one of type *A* and one of type *B*. The crystals used in this study had a vacancy concentration of 15% on the oxygen sublattice. If a homogeneous distribution of the vacancies is assumed, 66% of the vacancies will have no vacancy as next neighbor, while 33% will have exactly one next neighbor. Vacancies with more than one vacancy as next neighbor occur to less than 1% and are not taken into account. Therefore, the relative amounts of these microdomains can be fixed to 66% of type *A* and 33% of type *B*. Several refinements were calculated with different correlation schemes for the microdomains. These are listed in Table 1 together with the respective *R* factors.

Only the combination of a microdomain type based on a single vacancy (*A*I) and a microdomain type based on a pair of two vacancies separated by $a3^{1/2}/2$ along [111] with a cation in between (type *B*III) could reproduce the observed intensity distribution. To a single vacancy microdomain only those double-vacancy microdomains are correlated that are parallel to the orientation of the single-vacancy microdomain.

In order to obtain information about the reliability of the defect structure variations of the microdomain type *A* were considered. The model *A*II refined to an *R* factor of 34% and thus the relaxation of O(2) appears be along ⟨100⟩ as described by *A*I. In model *A*III, the relaxation of O(4) was modified to ⟨111⟩. The refinement resulted in an *R* factor of 31%. These calculations suggest that the microdomain *A*I correctly describes the relaxation directions of the displaced ions.

The model *A*IV allowed the composition of the microdomains to be verified. The calcium position of the microdomain *A*I was replaced by a zirconium ion. The refinement resulted in an *R* factor of 25%. The calculated intensity did not describe the observed intensity as well as the one for the model *A*I which resulted in an *R* factor of 27%. The difference intensity showed stronger deviations especially for scattering vectors apart from the peak intensities. These deviations are not taken into account for the calculation of the *R* factor. Furthermore, the positional parameter of the zirconium on the calcium site refined to a larger relaxation than the parameter of the other zirconium ions. This indicates that the microdomains preferentially contain one calcium. Since the difference in calculated intensities was only slight, the existence of microdomains that do not contain calcium cannot be fully excluded.

The model *A*I assumes relaxation of the second-nearest oxygen neighbors of the vacancy only for those oxygen ions that surround the calcium position. Since the refinement resulted in a relaxation of the zirconium ions away from the vacancy, relaxation of those second-nearest oxygen neighbors that surround the zirconium ions must be tested as well. Two refinements were carried out which allowed for relaxation of all second-nearest oxygen neighbors along ⟨101⟩ and ⟨111⟩, respectively. Both refinements did not result in a good agreement, the *R* factors were 33 and 37%, respectively. The oxygen ions did not relax significantly away from the ideal fluorite position.

Results

The single-vacancy microdomain appears to be of the type *A*I, the double-vacancy microdomain is of the type *B*III. The refined parameters are listed in Table 2. The weighted *R* value is 27% and the goodness of fit 3·9. Figs. 10 to 13 show the calculated intensities

Table 2. *Relaxations away from the ideal fluorite positions of the atoms within the microdomains*

Parameter	Relaxation (nm)	Standard deviation	
Microdomain of type *A*I			
O(1)	−0·006	±0·003	along ⟨100⟩
O(2)	0·016	±0·003	along ⟨100⟩
O(3)	0·012	±0·002	along ⟨111⟩
O(4)	0·010	±0·002	along ⟨101⟩
Zr	0·013	±0·002	along ⟨111⟩
Ca	0·030	±0·005	along ⟨111⟩
Microdomain of type *B*III			
O	0·041	±0·004	along ⟨100⟩
Metal	0·012	±0·006	along ⟨111⟩

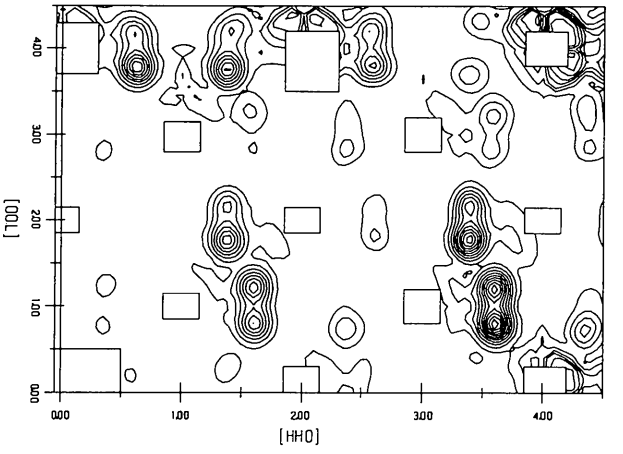

Fig. 10. Calculated intensity in the zero layer of the [1, −1, 0] zone, integral intensity, $T = 290$ K. The intensities are stepped with linear intervals of 50 counts, the lowest intensity represented is 100 counts. The Bragg reflections are represented by the rectangles.

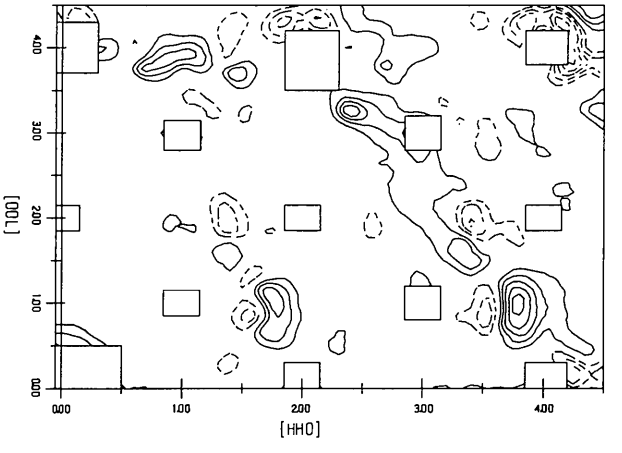

Fig. 11. Difference intensity $I_{obs} - I_{calc}$ in the zero layer of the [1, −1, 0] zone, integral intensity, $T = 290$ K. The intensities are stepped with linear intervals of 50 counts, the lowest intensities represented are 50 counts and −50 counts. The negative differences are represented by the broken lines. The Bragg reflections are represented by the rectangles.

and the difference intensities. All layers show good agreement of the observed and calculated data. All diffuse peaks are present in the calculated intensity distributions and show the correct intensities to a good agreement. Only two of the minor diffuse phenomena are not sufficiently explained. The intensity of the broad bands is calculated too low and the broadened shape of the diffuse peaks at (1·6, 1·6, 1·0) and (3·6, 3·6, 1·0) is not reproduced by the calculations.

The uncertainty of the relaxations listed in Table 2 varies from 10 to 45%. The positional parameter of O(I) shows the highest uncertainty of 45%. The negative value of the position parameter indicates a relaxation away from the vacancy, while the O(II) are relaxed towards the vacancy. Since the vacancy has a relative positive charge, a relaxation of the oxygen neighbors towards the vacancy should be expected. Since the relaxation of O(I) is only one third of that of O(II) and the uncertainty is high, no definite conclusion can be reached for the direction of the relaxation of O(I).

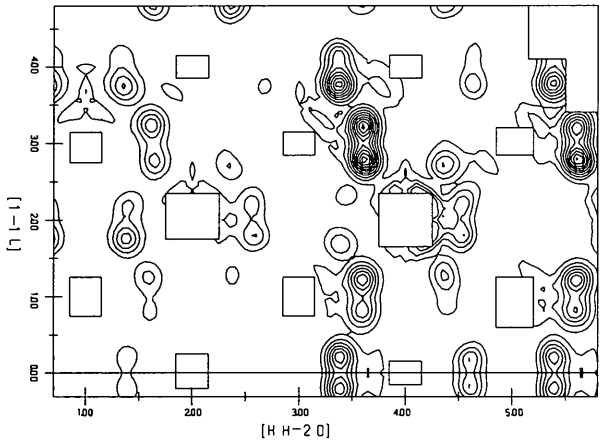

Fig. 12. Calculated intensity in the first layer of the [1, −1, 0] zone, integral intensity, $T = 290$ K. The intensities are stepped with linear intervals of 50 counts, the lowest intensity represented is 100 counts. The Bragg reflections are represented by the rectangles.

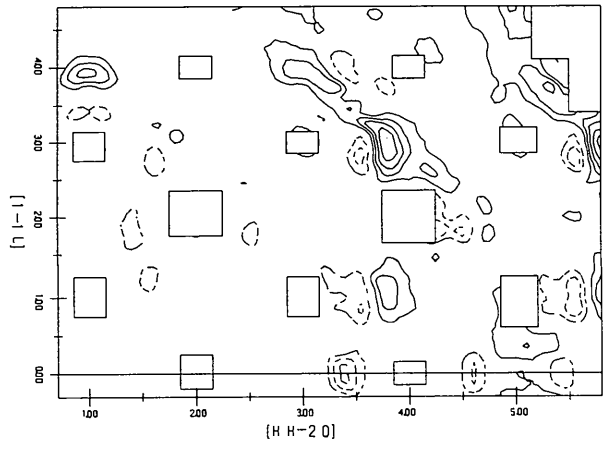

Fig. 13. Difference intensity $I_{obs} - I_{calc}$ in the first layer of the [1, −1, 0] zone, integral intensity, $T = 290$ K. The intensities are stepped with linear intervals of 50 counts, the lowest intensities represented are 50 counts and −50 counts. The negative differences are represented by the broken lines. The Bragg reflections are represented by the rectangles.

Table 3. *Interatomic distances within a microdomain of type AI*

	Distance (nm)
O(3)-Ca	0·204
O(3)-Ca	0·222
O(2)-Ca	0·227
O(1)-Zr	0·230
O(2)-Zr	0·219
O(3)-Zr	0·209
O(4)-Zr	0·218

The length of the relaxation of O(II) of 0·016 nm is in good agreement with values obtained by Morinaga, Cohen & Faber (1980) and Lorenz *et al.* (1988). The relaxation of the oxygen ions is twice as large as that of the zirconium.

The calcium ion is relaxed by a similar amount to the oxygen ions. Although O(III) and O(IV) are relaxed away from the calcium position, the bond lengths Ca–O(II) and Ca–O(III) (Table 3) are less than the sum of the ionic radii of 0·250 nm (Shannon, 1976). It can be expected that the second oxygen neighbors of the calcium ion are relaxed away from the calcium as well. A quantitative analysis of these relaxations could not be carried out owing to the large number of parameters.

The refinement showed that those second neighbors of the vacancy, which surround the zirconium, are not relaxed. The bond lengths Zr–O are in good agreement with the bond length of 0·222 nm in the ideal cubic zirconia structure.

Table 2 shows very large relaxations of the oxygens in the double-vacancy microdomain. In this microdomain type, relaxations were calculated only for the nearest oxygen neighbors. The relaxation of the zirconium ions is of the same value as that in the single-vacancy microdomain. Since no relaxation of second neighbors around the zirconium occurred in the single-vacancy microdomain, the model of the double-vacancy microdomain appears to be correct.

Calculations with single-vacancy microdomains that contained only zirconium did not show as good an agreement with the observed intensities as the calculation for a microdomain that contained one calcium. Furthermore, the position parameter of the zirconium on the calcium site refined to a longer relaxation than the parameter of the other zirconium. Thus it can be concluded that the microdomains preferentially contain one calcium. Since the difference in calculated intensities was only slight,

the existence of microdomains that do not contain calcium cannot be fully excluded.

Faber, Mueller & Cooper (1978) proposed a relaxation of the oxygen along ⟨100⟩ both for CSZ and YSZ. Andersen *et al.* (1985, 1986), too, found ⟨100⟩ for YSZ. Horiuchi *et al.* (1984), however, found both ⟨100⟩ and ⟨111⟩ for YSZ. Morinaga, Cohen & Faber (1979, 1980) describe only ⟨111⟩ for YSZ and CSZ. These contradictory results can be explained by the microdomain model presented in this study. The relaxation along ⟨100⟩ results from the relaxation of first neighbors of a vacancy, while relaxation along ⟨111⟩ results from relaxation of those second neighbors that surround the calcium in the single-vacancy microdomains.

Correlation of the single-vacancy microdomains was allowed only for microdomains that are parallel or at an angle of 54·7°. An explanation is offered by the dipole moment of the microdomain. The relaxation of the second neighbors shows that there are more extended displacement fields that will couple the microdomains. The number of vacany pairs is too small to result in any noticeable correlation between the double-vacancy microdomains. The diameter of these microdomains is roughly one unit cell which is too large for the correlation length.

Defect structure at 1550 K

At high temperature the intensity of only 30 diffuse peaks could be observed. Therefore, a complete analysis was not possible. Since there is little difference between the diffuse phenomena observed at room temperature and at 1550 K, the final model obtained at room temperature was used at high temperature. The small number of data did not allow the Debye–Waller factors to be refined. Fixed Debye–Waller factors were used that had been determined by Marxreiter (1988) from Rietveld refinements of neutron powder diagrams obtained with samples of identical origin.

The relaxations were fitted to the observed intensities of the purely elastic measurements.

The calculations of the diffuse intensity with the parameters obtained from the fit showed that a length of coherence shorter than that at room temperature was needed to describe the observed FWHM of the diffuse peaks and the observed intensity. However, the intensity of the general diffuse scattering was calculated too high. This could be corrected by reducing the relative number of the microdomains that are correlated. At room temperature all microdomains are distributed with correlations. At 1550 K only about 10% of the microdomains are correlated, while the other 90% are distributed at random.

Figs. 14 to 17 show the calculated and the difference intensity of the purely elastic and the integral measurements, the fitted parameters are listed in Table 4. The observed intensities are very well reproduced. Just the form of the calculated peaks is more symmetric than the observed form. Towards smaller 2θ the calculated intensity is too high, towards larger 2θ too low. The broad band of diffuse intensity from 440 to 224 is not described completely. The difference intensity plots, however, do not show any structured residual intensity.

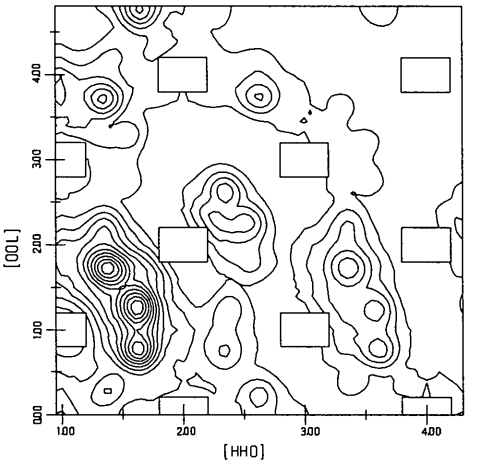

Fig. 14. Calculated intensity in the zero layer of the [1, −1, 0] zone, elastic intensity, $T = 1550$ K. The intensities are stepped with linear intervals of 10 counts, the lowest intensity represented is 20 counts. The Bragg reflections are represented by the rectangles.

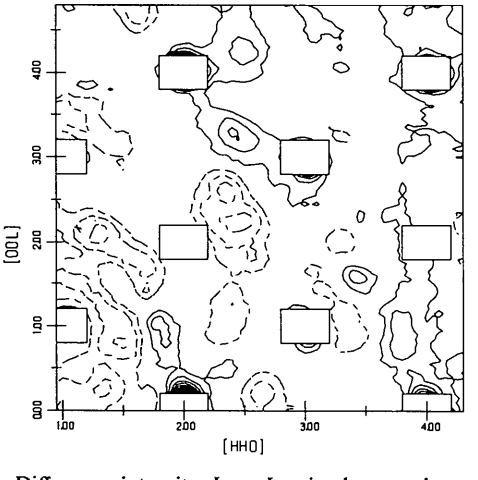

Fig. 15. Difference intensity $I_{obs} - I_{calc}$ in the zero layer of the [1, −1, 0] zone, elastic intensity, $T = 1550$ K. The intensities are stepped with linear intervals of 10 counts, the lowest intensities represented are 10 counts and −10 counts. The negative differences are represented by the broken lines. The Bragg reflections are represented by the rectangles.

Table 4. *Relaxation away from the ideal fluorite position of the atoms within the microdomains at* 1550 K

Parameter	Relaxation (nm)	Standard deviation	
Microdomain of type *AI*			
O(1)	0·016	±0·005	along ⟨100⟩
O(2)	Fixed		
O(3)	Fixed		
O(4)	Fixed		
Zr	0·011	±0·004	along ⟨111⟩
Ca	0·041	±0·012	along ⟨111⟩
Microdomain of type *BIII*			
O	Fixed		
Metal	Fixed		

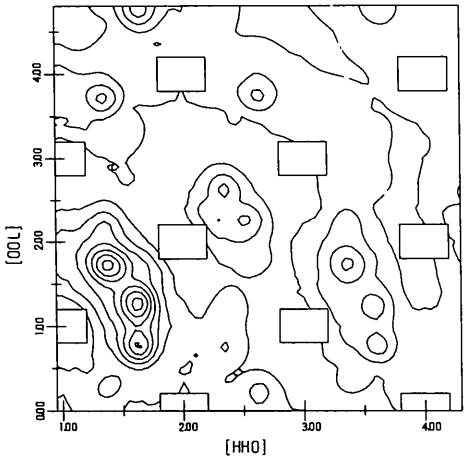

Fig. 16. Calculated intensity in the zero layer of the [1, −1, 0] zone, integral intensity, $T = 1550$ K. The intensities are stepped with linear intervals of 50 counts, the lowest intensity represented is 100 counts. The Bragg reflections are represented by the rectangles.

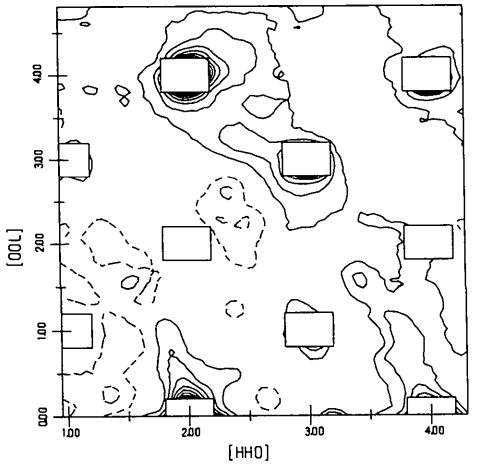

Fig. 17. Difference intensity $I_{obs} - I_{calc}$ in the zero layer of the [1, −1, 0] zone, integral intensity, $T = 1550$ K. The intensities are stepped with linear intervals of 50 counts, the lowest intensities represented are 50 counts and −50 counts. The negative differences are represented by the broken lines. The Bragg reflections are represented by the rectangles.

The uncertainties of the fitted parameters are fairly high. The only significant parameters are the O(1) and the cation positions in the single-vacancy microdomain. The other parameters show uncertainties larger than the refined value and were reset to zero. A detailed description of the structure of the microdomains at 1550 K thus is limited. The significant relaxations show the same values as at room temperature. The uncertainties of the other positional parameters are due to the small number of data points. Since the calcium is displaced significantly, relaxation of O(II) and O(III) and O(IV) should be expected. At high temperature the defect structure of CSZ consists of correlated microdomains identical to room temperature. Complete information on the relaxations is not available, the significant relaxations show the same values as at room temperature.

The comparison of the elastic and the integral measurements shows no significant changes in the difference intensity plots. For the integral calculations only a separate scale factor and background had been calculated. Thus, the initial observation that the defect structure of CSZ is of static nature is confirmed, or, at least, dynamic processes on a time scale higher than $0{\cdot}5 \times 10^{-11}$ s can be excluded.

Concluding remarks

The quantitative interpretation of diffuse neutron scattering has yielded an accurate description of the defect structure of calcium-stabilized zirconia at room temperature and at 1550 K. At room temperature, the defect structure can be described by a correlated distribution of two types of microdomains. These microdomains are coherently intergrown in the matrix of the disordered cubic crystal. The distribution of the microdomains shows short-range order with a correlation length of 0·52 nm or five times the d spacing of the (224) plane. The coherence length is about 2·0 nm. The two microdomains are based on vacancies of the oxygen site and relaxation of neighboring ions. The first type of microdomain is based on a single vacancy. The next-nearest oxygen neighbors are relaxed towards the vacancy along ⟨100⟩ by 0·016 nm. The calculations indicated that one of the cation neighbors appears to be calcium, which provides local charge balance. The calcium ion is relaxed away from the vacancy along ⟨111⟩ by 0·030 nm, while the zirconium ions are relaxed by 0·026 nm. The second type of microdomain is based on a pair of microdomains separated by $a3^{1/2}/2$ along [111]. Again, the next-nearest oxygen neighbors are relaxed towards the vacancy along ⟨100⟩ and the cations away from the vacancy along ⟨111⟩. This second type of microdomain is equivalent to the microdomain that Andersen *et al.* (1985) and Osborn *et al.* (1985) found in yttrium-stabilized zirconia. They did not report a microdomain based on a single vacancy.

The defect structure as described by the microdomain model does not consist of small precipitates of the Φ_1 phase. The intensities of the Φ_1 phase as observed by Marxreiter, Boysen, Frey & Vogt (1990) do not correspond to the intensities of the corresponding diffuse scattering. This confirms the results of Morinaga *et al.* (1980) who compared the intensities of the diffuse scattering with the intensity calculated from the partial structure model of the Φ_1 phase. The structure of the Φ_1 phase does not contain single oxygen vacancies. Furthermore, in the Φ_1 phase the calcium ions are second-nearest neighbors of the vacancies while they are preferentially nearest neighbors in the cubic solid solution.

This work was supported by funds of the BMFT.

References

ALLPRESS, J. G. & ROSSELL, H. J. (1975). *J. Solid State Chem.* **15**, 68-78.

ALLPRESS, J. G., ROSSELL, H. J. & SCOTT, H. G. (1975). *J. Solid State Chem.* **14**, 264-273.

ANDERSEN, N. H., CLAUSEN, K., HACKETT, M. A., HAYES, W., HUTCHINGS, M. T., MACDONALD, J. E. & OSBORN, R. (1985). *Proc. 6th Risø Int. Symp. on Metallurgy and Materials Science*, edited by F. W. POULSEN, N. H. ANDERSEN, K. CLAUSEN, S. SKAARUP & O. T. SORENSEN, pp. 279-284. London: Institution of Mining and Metallurgy.

ANDERSEN, N. H., CLAUSEN, K., HACKETT, M. A., HAYES, W., HUTCHINGS, M. T., MACDONALD, J. E. & OSBORN, R. (1986). *Physica (Utrecht)*, **136B**, 315-317.

BUTLER, V., CATLOW, C. R. A. & FENDER, B. E. F. (1983). *Radiat. Eff.* **73**, 273-277.

CARTER, R. E. & ROTH, W. L. (1963). In *Proc. Electromotive Force Measurements in High Temperature Systems*, edited by C. B. ALCOCK, pp. 125-144. London: Institution of Mining and Metallurgy.

FABER, J. JR, MUELLER, M. H. & COOPER, B. R. (1978). *Phys. Rev. B*, **17**, 4884-4888.

HELLMANN, J. R. & STUBICAN, V. S. (1983). *J. Am. Ceram. Soc.* **66**, 260-264.

HORIUCHI, H., SCHULTZ, A., LEUNG, P. C. W. & WILLIAMS, J. M. (1984). *Acta Cryst.* B**40**, 367-372.

HUDSON, B. & MOSELEY, P. T. (1976). *J. Solid State Chem.* **19**, 383-389.

HULL, S., FARLEY, T. W. D., HACKETT, M. A., HAYES, W., OSBORN, R., ANDERSEN, N. H., CLAUSEN, K., HUTCHINGS, M. T. & STIRLING, W. G. (1988). *Solid State Ionics*, **28–30**, 488-492.

KOESTER, L. & YELON, B. (1983). Neutron Diffraction Newsletter.

LORENZ, G. (1988). PhD thesis, Univ. München, Federal Republic of Germany.

LORENZ, G., FRAY, F., SCHULZ, H. & BOYSEN, H. (1988). *Solid State Ionics*, **28–30**, 497-502.

MARXREITER, J. (1988). Personal communication.

MARXREITER, J., BOYSEN, H., FREY, F. & VOGT, T. (1990). *Mater. Res. Bull.* **25**, 435-442.

MORINAGA, M., COHEN, J. B. & FABER, J. JR (1979). *Acta Cryst.* A**35**, 789-795.

MORINAGA, M., COHEN, J. B. & FABER, J. JR (1980). *Acta Cryst.* A**36**, 520-530.

NEDER, R. B., FREY, F. & SCHULZ, H. (1990). *Acta Cryst.* A**46**, 792-798.

OSBORN, R., ANDERSEN, N. H., CLAUSEN, K., HACKETT, M. A., HAYES, W., HUTCHINGS, M. T. & MACDONALD, J. E. (1985). *Mater. Sci. Forum*, **7**, 55-62.

SHANNON, R. D. (1976). *Acta Cryst.* A**32**, 751-767.

STEELE, D. & FENDER, B. E. F. (1974). *J. Phys. C*, **7**, 1-11.

SUBBARAO, E. C. (1981). In *Advances in Ceramics*, edited by A. H. HEUER & L. W. HOBBS, Vol. 3, pp. 1-24.

THORNBER, M. R., BEVAN, D. J. M. & GRAHAM, J. (1968). *Acta Cryst.* B**24**, 1183-1190.

Acta Cryst. (1990). A**46**, 809-820

Effect of the Anisotropy of Anomalous Scattering on the MAD Phasing Method

BY ERIC FANCHON* AND WAYNE A. HENDRICKSON

Howard Hughes Medical Institute, Department of Biochemistry and Molecular Biophysics, Columbia University, 630 West 168th Street, New York, New York 10032, *USA*

(*Received* 26 *January* 1990; *accepted* 22 *May* 1990)

Abstract

The analysis of X-ray diffraction intensities is complicated by the anisotropy of anomalous scattering (AAS) that can occur due to resonance associated with transitions between core electrons and valence molecular orbitals. Substantial AAS has been observed directly in diffraction data near the *K* edge of selenium in selenolanthionine [Templeton & Templeton (1988). *Acta Cryst.* A**44**, 1045-1051] and in pleiochroism of X-ray absorption in selenobiotinyl streptavidin [Hendrickson, Pähler, Smith, Satow, Merritt & Phizackerley (1989). *Proc. Natl Acad. Sci. USA*, **86**, 2190-2194]. The impact of AAS on the multiple-wavelength anomalous diffraction (MAD) method for phase determination is of particular interest in the context of this chemical state of selenium in the light of a general method that has been developed to incorporate selenomethionine into

* Present address: Laboratoire de Cristallographie, CNRS, 66X, 38042 Grenoble CEDEX, France.

0108-7673/90/100809-12$03.00